10-1-2023

Blocking the functional domain of TIP1 by antibodies sensitizes cancer to radiation therapy

Abhay K Singh

David Ya Dadey

Michael J Rau

James Fitzpatrick

Harendra K Shah

See next page for additional authors

Authors

Abhay K Singh, David Ya Dadey, Michael J Rau, James Fitzpatrick, Harendra K Shah, Minakshi Saikia, Reid Townsend, Dinesh Thotala, Dennis E Hallahan, and Vaishali Kapoor

Biomedicine & Pharmacotherapy 166 (2023) 115341

Contents lists available at ScienceDirect

Biomedicine & Pharmacotherapy

journal homepage: www.elsevier.com/locate/biopha

Blocking the functional domain of TIP1 by antibodies sensitizes cancer to radiation therapy

Abhay K. Singh [a], David YA Dadey [a,b], Michael J. Rau [c], James Fitzpatrick [c,d,e], Harendra K. Shah [a], Minakshi Saikia [a], Reid Townsend [f,g], Dinesh Thotala [a,g], Dennis E. Hallahan [a,g,*], Vaishali Kapoor [a,g,*]

[a] Department of Radiation Oncology, Washington University School of Medicine in St. Louis, St. Louis, MO, USA
[b] Department of Neurosurgery, Stanford University School of Medicine, Stanford, CA, USA
[c] Center for Cellular Imaging, Washington University School of Medicine in St. Louis, St. Louis, MO, USA
[d] Departments of Cell Biology & Physiology and Neuroscience, Washington University School of Medicine, St. Louis, MO, USA
[e] Department of Biomedical Engineering, Washington University in St. Louis, St. Louis, MO,USA
[f] Department of Medicine, Washington University in St. Louis, St. Louis, MO,USA
[g] Siteman Cancer Center, St. Louis, MO, USA

ARTICLE INFO

Keywords:
Radiation therapy
Therapeutic target
Antibody
Lung cancer
Glioblastoma
TIP1

ABSTRACT

Non-small-cell lung cancer (NSCLC) and glioblastoma (GB) have poor prognoses. Discovery of new molecular targets is needed to improve therapy. Tax interacting protein 1 (TIP1), which plays a role in cancer progression, is overexpressed and radiation-inducible in NSCLC and GB. We evaluated the effect of an anti-TIP1 antibody alone and in combination with ionizing radiation (XRT) on NSCLC and GB in vitro and in vivo. NSCLC and GB cells were treated with anti-TIP1 antibodies and evaluated for proliferation, colony formation, endocytosis, and cell death. The efficacy of anti-TIP1 antibodies in combination with XRT on tumor growth was measured in mouse models of NSCLC and GB. mRNA sequencing was performed to understand the molecular mechanisms involved in the action of anti-TIP1 antibodies. We found that targeting the functional domain of TIP1 leads to endocytosis of the anti-TIP1 antibody followed by reduced proliferation and increased apoptosis-mediated cell death. Anti-TIP1 antibodies bound specifically (with high affinity) to cancer cells and synergized with XRT to significantly increase cytotoxicity in vitro and reduce tumor growth in mouse models of NSCLC and GB. Importantly, downregulation of cancer survival signaling pathways was found in vitro and in vivo following treatment with anti-TIP1 antibodies. TIP1 is a new therapeutic target for cancer treatment. Antibodies targeting the functional domain of TIP1 exhibited antitumor activity and enhanced the efficacy of radiation both in vitro and in vivo. Anti-TIP1 antibodies interrupt TIP1 function and are effective cancer therapy alone or in combination with XRT in mouse models of human cancer.

1. Introduction

Non-small-cell lung cancer (NSCLC) and glioblastoma (GB) are two of the most lethal malignancies. While novel approaches to therapy and diagnosis have yielded modest improvements in survival, the 5-year overall survival of patients with NSCLC or GB is approximately 15% and 5 %, respectively [1,2]. Thus, there is an unmet need for more effective treatments for NSCLC and GB [3].

One potential approach involves molecular targeted therapy. Numerous targets, including EGFR, ALK, and VEGFR, are of significant interest due to the notion of inducing specific cytotoxicity in NSCLC and GB [4,5]. However, there have been limited improvements in therapeutic efficacy with these molecular targets. Tax interacting protein 1 (TIP1) is a molecular target that was discovered through in vivo phage display biopanning. TIP1 is expressed on the surface of cancer cells and induced during radiation therapy [6–9].

The functional domain of TIP1 is the PSD-95/DlgA/ZO-1 (PDZ) domain. PDZ domain-containing proteins are involved in cell signaling events and membrane protein trafficking in cancer [10]. PDZ domains usually span 80–100 amino acid residues and contain six β-sheets and

* Corresponding authors at: Department of Radiation Oncology, Washington University School of Medicine in St. Louis, St. Louis, MO, USA
E-mail addresses: dhallahan@wustl.edu (D.E. Hallahan), vkapoor@wustl.edu (V. Kapoor).

https://doi.org/10.1016/j.biopha.2023.115341
Received 25 June 2023; Received in revised form 11 August 2023; Accepted 19 August 2023
Available online 23 August 2023

two α-helices. PDZ domains recognize a specific C-terminal sequence motif in their target proteins [11]. Most PDZ domain-containing proteins have several PDZ domains. TIP1 is unique since it consists of a single PDZ domain encompassing residues 13–112 of the 124-amino acid protein. It recognizes proteins containing an X-S/T-X-I/L/V--COOH C-terminal recognition motif and a recently identified -S/T-X-L/V-D- internal motif [11].

TIP1 interacts with numerous proteins that regulate cell viability, including PLC, PKC, FAS, and Rho [12–15]. It has also been identified as an essential molecule for cancer cell migration, adhesion, and metastasis [16,17]. Our previous work found that TIP1 levels correlated with progression and poor prognosis in several cancers [6]. Furthermore, TIP1 contributes to resistance to radiation therapy [18]. Despite these findings that TIP1 contributes to cancer cell survival, little is known about the role of TIP1 at the cell surface.

In the present study, we investigated the use of antibody-mediated targeting of the PDZ domain of TIP1 and its effect on the efficacy of radiation in NSCLC and GB. We found that cancer-specific targeting and cytotoxicity can be achieved using antibodies against the PDZ domain of TIP1, both in vitro and in vivo. Mechanistically, we found that blocking the PDZ domain of TIP1 modulates cell survival pathways that ultimately lead to cytotoxicity. Our findings suggest that TIP1 is a potential target for drug development in NSCLC, and GB and antibody-mediated targeting of TIP1 at the cell surface may represent a new strategy to enhance the efficacy of radiation therapy.

2. Materials and methods

2.1. Cell lines, chemicals, and irradiation

The human glioblastoma cell line D54 was a gift from Dr. Yancey Gillespie (the University of Alabama at Birmingham). The human U251 glioblastoma cell line was obtained from the NCI. Human NSCLC cell lines A549 and H460 were obtained from ATCC. Mouse NSCLC cell line LLC and mouse glioblastoma cell line GL261 were obtained from ATCC. MRC-5 cell line was purchased from Sigma (St. Louis, MO). D54, LLC, GL261, and A549 cells were cultured in DMEM/F-12; U251 and H460 were cultured in RPMI media containing 10 % fetal bovine serum (FBS) and 1 % penicillin-streptomycin (P/S). MRC-5 were grown in EMEM media supplemented with 1% Penicillin and Streptomycin, 10% fetal bovine serum, non-essential amino acids, and glutamax. All cell cultures were grown in a humidified incubator at 37 °C with 5 % CO_2. Cells lines were authenticated by short-tanderm repeat (STR) profiling at the Washington University's McDonnell Genome Institute. All the cell lines were tested for mycoplasma contamination using the MycoAlert™ PLUS Mycoplasma Detection Kit (Lonza) every three months and tested negative. All cell lines were disregarded after 15 passages from thawing. For in vivo injections, cells were used within 10 passages from thawing. Ionizing radiation was delivered using an x-ray irradiator (RS 2000, Rad Source, USA) with an operating voltage and current of 160 kV and 25 mA, respectively. A dose rate of 0.0682 Gy/s and 0.0167 Gy/s was used for in vitro and animal radiation experiments, respectively. Mice were anesthetized with 2 % isoflurane and placed in the irradiator with shielding of the body using lead. The target tissues (hindlimb tumors) were exposed during radiation for animal experiments.

2.2. Antibodies

The anti-TIP1 antibody that specifically binds to the PDZ domain (anti-PDZ/TIP1 antibody) was obtained from Santa Cruz. The antibody that binds outside the PDZ domain (anti-non-PDZ/TIP1 antibody), 2C6F3, was produced and characterized by us earlier [12]. The phospho-Akt (S473), total Akt, phospho-mTOR (S2448), total mTOR, phospo-P70S6 (T389) total-P70S6 phospo-4EBP1 (T70), 4EBP1 (T70) and GAPDH antibodies were purchased from Cell Signaling Technologies.

2.3. Structural representation of anti-PDZ/TIP1 epitope on the 3D structure of TIP-1

The location of the epitopes of the anti-PDZ/TIP1 antibody and non-PDZ antibody was overlaid on the already published crystal structure of TIP1, 3DIW [19]. PyMOL software was used to overlay the epitopes of the anti-PDZ/TIP1 antibody and non-PDZ antibody on the 3D structure of TIP1.

2.4. Gel filtration

The anti-TIP1 antibody was incubated with purified TIP1 protein in vitro and subjected to gel filtration chromatography with a Superdex S200 10/300 GL column (GE Healthcare) in phosphate-buffered saline. The molecular weight was estimated from a calibration curve that was prepared by using the standard proteins (Biorad). The complex formation was evaluated by SDS-PAGE and western blotting. The gel-filtered anti-TIP1 antibody in complex with TIP1 protein was used for negative stain transmission electron microscopy.

2.5. Negative stain transmission electron microscopy

For negative stain transmission electron microscopy (TEM), samples were prepared on continuous carbon films supported on 200 mesh copper grids. 10 μl drops of gel-filtered anti-TIP1 antibody in complex with TIP1 was applied to the grid to incubate for 1 min. Post-incubation, the grid was washed (5 times) with ddH20, washed once with 0.75% uranyl formate (1 drop), and stained with 0.75 % uranyl formate for 3 min. The preparation was then blotted using filter paper, leaving a small amount of stain to air dry on the grid surface. Grids will then be imaged on a JEOL 1400 TEM equipped with an AMT CCD camera operating at 120 kV. Micrographs were collected at 100,000x magnification at a defocus value of ranging from 1.5 to 2 μm. 30 individual micrographs were obtained, which were subsequently processed using the RELION 2.1 software package to perform 2D class averaging. Ten classes were extracted using approximately 9000 individual particles.

2.6. Surface plasmon resonance (SPR)

The affinity of the anti-TIP1 antibody for TIP1 protein was measured by the biosensor-based surface plasmon resonance (SPR) technique using an automatic apparatus BIAcore 2000 (GE Healthcare, Sweden) as we described earlier [20–22]. The recombinant TIP1 protein (Prospec, USA) was immobilized by amine coupling on the CM4 sensor surface (ligand), and the anti-TIP1 antibody was used as the analyte. Experiments were performed at 25 °C in HBS-EP buffer (GE healthcare). TIP1 protein was immobilized using surface preparation wizard for amine coupling. Briefly, equal volume (115 μl) of N-hydroxysuccinimide (NHS, 2.3 mg in 200 μl of water) and N-ethyl-N′− 3 (diethylamino propyl) carbodiimide (EDC, 15 mg in 200 μl of water) was mixed, and 75 μl of this solution was injected into the flow cell at the flow rate of 5 μl/min across the CM4 sensor chips to activate the carboxymethylated dextran surface for 15 min. TIP1 protein (50 μg/ml in 10 mM sodium acetate, pH 4.7) was injected at the flow rate of 5 μl/min across the activated surface for 25 min. The residual NHS esters were inactivated with ethanolamine (50 μl) for 10 min. A blank reference surface was also prepared with the same procedure by activation with EDC/NHS and then inactivation with ethanolamine. The affinity of the interaction was determined from the level of binding at equilibrium as a function of the sample concentrations by BIA evaluation software 3.0. The rate constant K_D was obtained by fitting the sensogram data after reference subtraction (data from the blank channel) using the BIA evaluation 3.0 software.

2.7. Cell proliferation assays

Cells (A549, H460, U251, and D54) were seeded at a density of

10,000 cells/well in 12 well plates and treated with 1 μg/ml of anti-PDZ/TIP1 antibody or isotype antibody as control and allowed to incubate for 24 h, 48 h, 72 h, and 96 h. The cells were then trypsinized and counted using a ViCell cell viability analyzer (Beckman Coulter). Cell proliferation was calculated as percentage: 100 *Cell number at each time point/cell number at 0 h. Three independent experiments having triplicates for each treatment were performed for each cell line.

2.8. CRISPR/Cas9 mediated knockout of TIP1

We performed CRISPR/Cas9 mediated knockout of TIP1, as previously described [23]. Briefly, two different guide RNAs (sgRNA 2: CCAGGGTATTTATGTCACAC and 3: CATTGGAGGTGGAATCGACC) were cloned into the pLentiCRISPRV2 vector. An unmodified vector was used as the CRISPR control in all experiments. After validation of the insertion by sequencing, lentivirus-mediated transduction of A549 and U251 cells was performed. Cells were selected with puromycin, and stable clones were validated for knockout of TIP1 by western blots.

2.9. Antibody internalization assays by live-cell imaging

A549 cells were seeded into glass-bottom chamber slides (Mattek) in phenol red-free medium. The following day, cells were stained with a cell mask orange dye (Invitrogen) as per the manufacturer's instructions. The cells were then treated with Alexa-Flour 488 labeled anti-PDZ/TIP1 antibody and visualized using a spinning disk confocal microscope (Nikon Eclipse Ti-E). Z-stack live cell images were captured every 5 min, and the acquisition was continued for 24 h.

2.10. Annexin V apoptosis assay

Cells (A549, H460, U251, and D54) were treated with 1 μg/ml anti-PDZ/TIP1 antibody or isotype control and incubated for 96 h. The cells were collected 96 h post-treatment and stained with Annexin V-FITC and PI (BD Biosciences) as per the manufacturer's protocol. The cells were analyzed for apoptosis by flow cytometry using a MACSQuant Analyzer (Miltenyi Biotech). For assays with Fas ligand (e-Biosciences), cells were treated with 50 ng/ml Fas ligand in combination with 1 μg/ml anti-PDZ/TIP1 antibody and evaluated for apoptosis by Annexin V assay.

2.11. Western immunoblot analysis

Cells (A549, H460, U251, and D54) were treated for 96 h with 1 μg/ml anti-PDZ/TIP1 antibody or isotype control and then lysed using M-PER mammalian protein extraction reagent (Thermo-Fisher Scientific). Protein extracts were blotted and probed using antibodies against phospho-AKT (Ser 473), total-AKT, phospho-mTOR (Ser 2448), total-mTOR, phospho-p70S6 kinase, total-p70S6 kinase, phospho-4EBP1, total-4EBP1 (Cell Signaling Technology). To evaluate protein loading, the blots were probed for GAPDH (Cell Signaling Technology). The blots were visualized using the ChemiDoc-MP Imaging System (Bio-Rad) and analyzed with Image Lab Software (Bio-Rad).

2.12. Colony formation assays

Cells (A549, H460, U251, and D54) were treated with 1 μg/ml anti-PDZ/TIP1 antibody or isotype control and allowed to incubate for 96 h. Cells were then sub-cultured in six-well plates and irradiated with 0, 1, 3, 5, and 7 Gy. The plates were incubated for 7–10 days following irradiation, and the colonies were stained with 0.5% crystal violet. Colonies consisting of 50 or more cells were counted using a StemiVD4 dissecting microscope (Zeiss). The survival fractions were calculated after normalizing to the plating efficiency of the unirradiated isotype control [24]. The impact of co-treatment of antibody with radiation was assessed by calculating sensitivity enhancement ratios (SER) at 3 Gy, 5 Gy, and 7 Gy. The sensitivity enhancement ratio at 3 Gy ($SER_{3\ Gy}$) is defined as the ratio of cell survival without and with anti-PDZ/TIP1 antibody at 3 Gy. Three independent treatments were performed for each cell line.

2.13. Immunohistochemistry

Immunohistochemistry for lung cancer (Origene) and normal tissue microarray (Biochain) was performed using standard procedures. Briefly, TMA sections were de-waxed in xylene and then rehydrated in a graded alcohol series. Antigen retrieval was performed by immersing the slides in Tris-EDTA buffer (10 mM, pH 9.0) for 10 min at 125 °C in a pressure cooker. Endogenous peroxidase activity was blocked with 3 % hydrogen peroxide in methanol for 30 min. Non-specific binding sites were blocked by 5 % normal goat serum for 1 h. Slides were incubated with anti-TIP1 antibody (dilution 1:100; Abcam) overnight at 4 °C in a wet chamber. Slides were washed with phosphate-buffered saline-tween 20 (0.01 %) (PBST) and then incubated with anti-rabbit HRP conjugated secondary antibody (1:5000; Sigma) for 1 h at room temperature in a wet chamber. After washing with PBST, the color was developed with a solution of 0.03 % diaminobenzidine for 2 min at room temperature, and the sections were counterstained with hematoxylin.

2.14. RNA-Seq

Cells were treated with the anti-TIP1/PDZ antibody for 0, 12, 24, and 36 h. The mRNA was isolated from these cells using the miRVANA kit (Ambion). RNA sequencing was performed by Genome Technology Access Center (GATC), Washington University in St. Louis. RNA-Seq reads were aligned to the Ensembl release 76 top-level assembly with STAR version 2.0.4b. Gene counts were derived from the number of uniquely aligned unambiguous reads by Subread: feature count version 1.4.5. Transcript counts were produced by Sailfish version 0.6.3. Sequencing performance was analyzed for a total number of aligned reads, the total number of uniquely aligned reads, genes, and transcripts detected, the ribosomal fraction is known junction saturation and read distribution over known gene models with RSeQC version 2.3.

All gene-level and transcript counts were then imported into the R/Bioconductor package EdgeR, and TMM normalization size factors were calculated to adjust samples for differences in library size. Genes or transcripts not expressed in any sample or less than one count-per-million in the minimum group size minus one were excluded from further analysis. The TMM size factors and the matrix of counts were then imported into R/Bioconductor package Limma, and weighted likelihoods based on the observed mean-variance relationship of every gene/transcript and sample were then calculated for all samples with the voom Quality Weights function. The performance of the samples was assessed with a Spearman correlation matrix and multi-dimensional scaling plots. Gene/transcript performance was evaluated with plots of the residual standard deviation of every gene to their average log-count with a robustly fitted trend line of the residuals. Generalized linear models were then created to test for gene/transcript-level differential expression. Differentially expressed genes and transcripts were then filtered for FDR adjusted p-values less than or equal to 0.05.

2.15. Quantitative proteomic analysis

Briefly, the anti-PDZ/TIP1 antibody-treated cells were solubilized, and the peptides were labeled with tandem mass tag reagents (TMT10). The Nano-LC-MS/MS analysis was done using a PepMap 100 C18 RSLC column (Thermo-Fisher Scientific) on an EASY nanoLC (Thermo Fisher Scientific). The proteins were quantitated using the intensities of MS2 reporter ions across the ten TMT channels. To associate signals across TMT multiplexes, common reference material was pooled from all the samples. The intensities and ratios of peptides were calculated using the means of the top-n entries of PSMs ordered from high to low reporter-ion intensity. Biological or technical differences between samples and

references were offset by measuring the medians from true biological medians. A cut-off at 1.5 ×CV was used as a QC filter to guard against outliers for further analysis (see equipment for more details). Heat-map visualization of peptide and protein log2-ratios was performed using the web-based tool Morpheus (https://software.broadinstitute.org/morpheus).

2.16. In-vivo near-infrared imaging

The TIP-1 antibody or isotype control antibody was labeled with IRDye 800CW as per manufacturer's instructions (Licor). Tumors were induced by injecting A549 (1×10^6) or U251 (0.5×10^6) cells in the right hind limbs of nude mice. The tumors were irradiated with three fractions of 3 Gy or 0 Gy (sham) separated by 8 h for 24 h. The tumor-bearing mice were then injected with 10 μg of labeled antibodies via the tail vein. For optical imaging, the mice were anesthetized with 2 % isoflurane and imaged using the Pearl Trilogy small animal imaging system (Li-cor). Fluorescence was detected using an 800 nm channel with excitation of 785 nm and an emission of 820 nm. Animals were imaged at 0, 3, 6, 24, 48, and 72 h following antibody injection. Images were analyzed using the Image Studio software (Licor). Background subtracted signal intensity that was normalized by tumor volumes of each mouse was plotted using Graph Pad Prism software.

2.17. qRT-PCR

mRNA expression of TIP1 was evaluated in H460 tumors. The tumors implanted in nude mice were irradiated with three fractions of 3 Gy or 0 Gy (sham) separated by 8 h for 24 h. Tumors were harvested 24, 48, and 72 h after the last dose of XRT and total RNA extracted using the RNAeasy kit (Qiagen). 1 μg of isolated total RNA samples were reverse-transcribed to cDNA as per manufacturer's instructions (Applied biosystems). The resulting cDNA was then used for quantitative real-time PCR amplification. qRT-PCR was performed by Taqman assay (ThermoFisher scientific) for TIP1 (NCBI Ref Seq: NM_001204698.1) and normalized by GAPDH (NCBI Ref Seq: NCBI Reference Sequence: NM_001256799.2) and beta-Actin (NCBI Ref Seq: NCBI Reference Sequence: NM_001101.3) housekeeping genes. The results were analyzed by the $2^{-\Delta\Delta CT}$ method.

2.18. Tumor growth delay

All animal studies were performed per the guidelines of the IACUC and with protocols approved by the Washington University Division of Comparative Medicine. Heterotopic tumor models were established by injecting A549 (3×10^6) and U251 (1×10^6) cells subcutaneously into the hind limbs of 6–8 week-old female athymic nude mice (Envigo, USA). The tumor-bearing mice were serpentine sorted by tumor volume and distributed into four groups having five mice, each with an average tumor volume of 200 mm^3. The treatment groups were as follows: (a) isotype control antibody; (b) isotype control antibody combined with XRT; (c) anti-PDZ/TIP1 antibody; and (d) anti-PDZ/TIP1 antibody combined with XRT. The tumors in XRT groups were irradiated with 2 Gy per day for five consecutive days while shielding the rest of the body with lead. The antibodies were injected via the tail vein on days 1 and 4 of the treatment. The tumor volumes were measured using a digital caliper on the indicated days. Mouse body weights were measured at each time point. Kaplan-Meier survival curves were used to determine the efficacy of combining the antibodies with radiotherapy. The humane endpoint was used as the criteria to sacrifice each mouse when tumors reached a volume of 2000 mm^3.

2.19. Statistical analysis

Statistical analyses were performed using the Student's *t*-test and or one-way or two-way analysis of variance (ANOVA). Bonferroni's multiple comparisons test was applied where necessary. These analyses were performed using Prism 6 (GraphPad Software, La Jolla, CA, USA), and statistical significance is indicated in each graph where appropriate. For in vitro experiments, we estimated that the minimum detectable difference between treatment groups is approximately 15% with a standard deviation of approximately 2.5 %. Utilizing this information, we achieve approximately 84 % power with an alpha of 0.05 utilizing 3 samples per treatment group. The tumor growth data were analyzed using Tukey's' multiple comparisons. Statistical analysis for Kaplan-Meier survival curves was performed using the Log-rank (Mantel-Cox) test. Number of mice per group was estimated using power analysis based on our previous study [25]. With 10 mice per group and an estimated standard deviation of 5 days, we achieve 88% power to detect a significantly greater delay in tumor growth with the anti-PDZ/TIP1 antibody treatment with a pairwise error rate of approximately 0.05.

3. Results

3.1. TIP1 is overexpressed and correlates with poor survival in NSCLC and GB

We correlated the expression of TIP1 with overall survival (OS) and disease-free survival (DFS) in patients with lung adenocarcinoma, lung squamous cell carcinoma, and GB. We analyzed the Cancer Genome Atlas (TCGA) and Genotype-Tissue Expression (GTEx) RNA-Seq data for cancer and healthy tissue using the web-based Gene Expression Profiling Interactive Analysis (GEPIA) [26]. We found a significant relationship between high TIP1 levels and poor overall survival in lung adenocarcinoma (HR 1.5, $p = 0.0077$) (Fig. 1A), lung squamous cell carcinoma (HR 1.3, $p = 0.045$) (Fig. 1B) and GB (HR 1.8, $p = 0.0015$) (Fig. 1C). Low TIP1 levels correlated with disease-free survival in GB (HR 1.5, $p = 0.053$) (Fig. 1D).

We evaluated TIP1 expression in NSCLC patients using a tumor tissue microarray (TMA) containing NSCLC tumors and matched healthy lung tissue (Fig. 1E). We found high expression of TIP1 in NSCLC tumors, and no expression in matched healthy tissues. To evaluate TIP1 as a cancer-specific target for drug development, we evaluated TIP1 expression in healthy tissues using immunohistochemistry in a normal TMA (Fig. 1F). No expression of TIP1 was found in any of the organs on the TMA (Fig. 1F).

3.2. TIP1 is radiation inducible

TIP1 is a radiation-inducible antigen [9,27,28]. We evaluated the radiation-inducible expression of TIP1 in cancer cells and mouse models of NSCLC and GB. TIP1 is overexpressed on the surface of cancer cells 24 and 48 h following three doses of 3 Gy irradiation (Supplementary Fig. 1A). TIP1 mRNA expression was evaluated in NSCLC tumors harvested from nude mice 24, 48, and 72 h after irradiation and compared to the sham irradiated tumors (Supplementary Fig. 1B). The fold-change in TIP1 mRNA expression was 3.6 ± 1.2, 5.0 ± 2.0 ($p < 0.01$), and 1.99 ± 0.5 24, 48, and 72 h after XRT respectively (Supplementary Fig. 1B). TIP1 protein expression in mouse models of cancer was evaluated by treating A549 (NSCLC) or U251 (glioma) tumor-bearing mice with an anti-TIP1 antibody labeled with IR Dye800. Nude mice bearing heterotopic A549 and U251 tumors on the right hind limbs were imaged with near-infrared (NIR) imaging over several days (Fig. 2A and Supplementary Fig. 1C). We found TIP1 upregulation in A549 and U251 tumors following irradiation (Fig. 2A-C and Supplementary Fig. 1C, D). In A549 tumors, a significantly higher ($P < 0.01$) normalized NIR signal intensity of the anti-TIP1 antibody was observed following irradiation with three doses of 3 Gy (3.5 ± 0.4 at 24 h, 4.1 ± 0.7 at 48 h) compared to the isotype control (0.5 ± 0.1 at 24 h, 0.6 ± 0.1 at 48 h) (Fig. 2B, C). In U251 tumors, a significantly higher ($P < 0.01$) TIP1 expression was observed 24 h after irradiation with three doses of 3 Gy (2.3 ± 0.4) compared to the sham-irradiated tumors (1.0 ± 0.1) (Supplementary

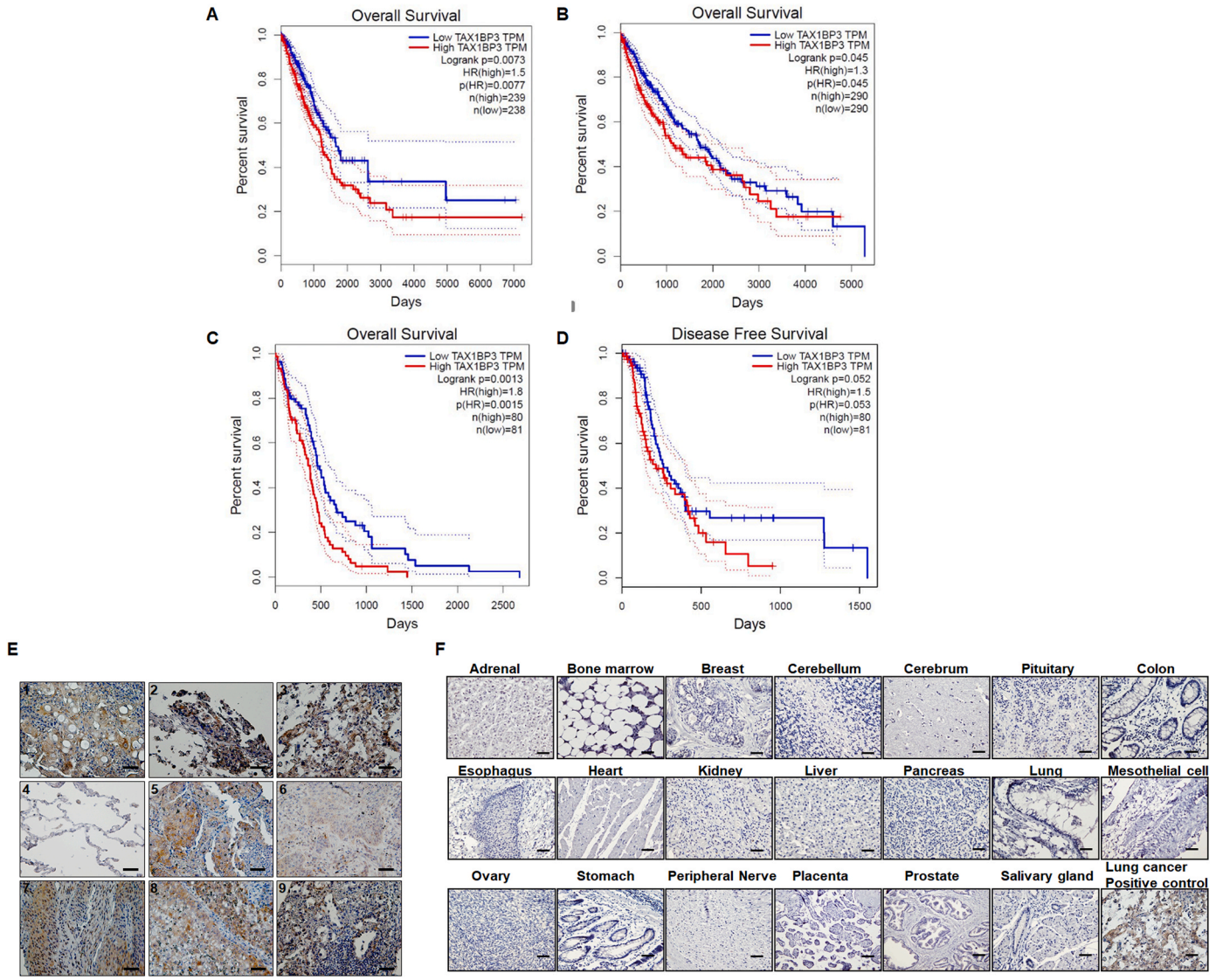

Fig. 1. TIP1 is overexpressed in NSCLC and GB and correlates to poor survival. (A-D) Kaplan–Meier survival curves showing overall survival of lung cancer patients grouped according to their TIP1 expression levels. The survival curves were generated using the GEPIA web-browser by analyzing the TCGA RNA-Seq dataset. A: Lung adenocarcinoma, B: Lung squamous cell carcinoma, C: Glioblastoma, D: Disease-free survival for glioblastoma. (E) Lung cancer tissue array showing the expression of TIP1 in lung cancers from patients. Panel 4 shows a matched healthy lung tissue showing no expression of TIP1 in normal lungs. Scale bar (black) in the bottom right corner is 50 μm. (F) Immunohistochemistry for TIP1 expression in healthy tissue array. Shown are microscopic photos of IHC stain with the anti-TIP1 antibody on 20 different healthy tissues showing no TIP1 expression and a lung cancer positive control showing intense TIP1 staining. Scale bar (black) in the bottom right corner is 50 μm.

Fig. 1D). The difference between the normalized NIR signal intensities of the anti-TIP1 antibody and isotype control was not statistically significant in sham irradiated tumors (Fig. 2B, C).

We next evaluated the intensity of TIP1 expression in the harvested tumors by immunofluorescence. Higher TIP1 staining intensity was observed in the irradiated tumor tissues compared to the sham irradiated control tumors (Fig. 2D). We also evaluated the ability of the anti-TIP1 antibody to target orthotopic brain and lung tumors (Supplementary Figs 1E and F). We injected luciferase-expressing U251 cells into the brains (Supplementary Fig. 1E) and lewis lung carcinoma (LLC) cells in the lungs of mice (Supplementary Fig. 1F). Bioluminescence imaging detected the tumors in the right brain and lungs, respectively. The anti-TIP1 antibody labeled with IR Dye 800 was injected via tail vein, and NIR imaging was performed. Supplementary Fig. 1E shows the localization of the anti-TIP1 antibody in the brain tumor. Supplementary figure 1 F shows that the antibody detected tumors in the lung, but not the surrounding healthy tissues. Specific tumor binding of the anti-TIP1 antibody was also observed in the excised organs (Supplementary Fig. 1E). We evaluated cell surface TIP1 expression following radiation in normal lung fibroblasts MRC5 by flow cytometry (Supplementary Fig. 1G). Radiation therapy did not induce TIP1 on the surface of MRC5 cells.

3.3. *Blocking the PDZ pocket of TIP-1 attenuates cell proliferation*

While developing radioimmunoconjugates against TIP1 [12], we serendipitously discovered that antibodies targeting the PDZ (functional) domain of TIP1 attenuate cancer cell proliferation. To determine whether the functional domain of TIP1 plays a role in this effect, we treated the NSCLC and GB cells with two different anti-TIP1 antibodies (Ab1 and Ab2). We first mapped the epitopes of these antibodies and then performed *in silico* modeling to determine that the proliferation attenuation is due to blocking of the functional domain of TIP1. We used PYMOL software to depict the 3D surface structure of the TIP1 protein

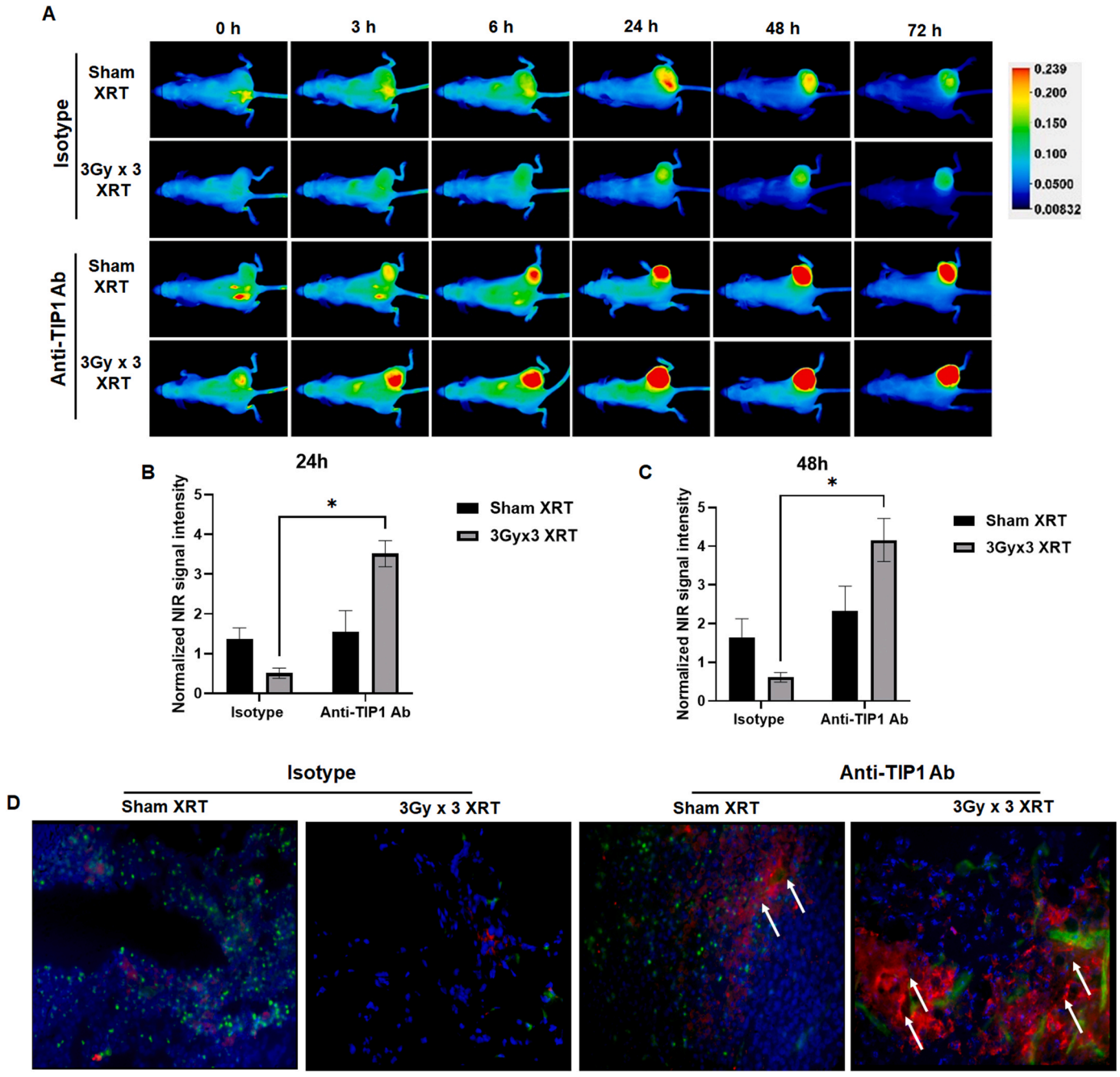

Fig. 2. TIP1 is a radiation-inducible target for cancer. Near-infrared imaging in nude mice bearing heterotopic A549 tumors in the right hind limb. Mice were injected with 10 ug IRDyee 800 labeled anti-PDZ/TIP1 antibody or isotype control via tail vein and imaged using a Pearl Trilogy (Licor) instrument at the indicated time points. Tumors were irradiated with three fractions of 3 Gy irradiation for 24 h before antibody injection, while "sham" treated mice received 0 Gy. Shown are representative images from each group. (B) Bar graphs showing near-infrared signal intensity as obtained after background subtraction and normalization with tumor volumes for sham irradiated and 3 Gy x3 irradiated tumors injected with the anti-TIP1 Ab or isotype control at 24 h. (C) Bar graphs showing near-infrared signal intensity as obtained after background subtraction and normalization with tumor volumes for sham irradiated and 3 Gy x3 irradiated tumors injected with the anti-TIP1 Ab or isotype control at 48 h. Mean, and SD has been plotted for each group. *p,0.05, * *p < 0.01, * *p,0.001 (D) Fluorescent microscopy of A549 tumor sections showing expression of TIP1 following irradiation. Red: TIP1 staining with anti-rabbit antibody, green: CD31 for endothelial cells, blue: DAPI.

and identified the epitopes of Ab1 and Ab2 (Supplementary Fig. 2A). Interacting partners bind to TIP1 in the groove of the PDZ domain that lies between the β2-strand and α2-helix [11] (white arrows, Supplementary Fig. 2A). The PDZ binding domain in TIP1 contains a short β-hairpin composed of two antiparallel β-strands (βa and βb) which are critical for ligand binding and are absent in other PDZ domain-containing proteins [11]. The first epitope of the Ab1 spans βa and βb, the loop between βa and βb, the Isoleucine (I), leucine (L), glycine (G) and phenylalanine (F) motif (ILGF), β2, and the loop following β2 (Supplementary Fig. 2A top panels). The second epitope spans the end of α1 containing the loop region followed by β4 (Supplementary Fig. 2A top panels). Ab1 is designated as an anti-PDZ/TIP1 antibody. A similar representation of the epitope of the Ab2 indicated that this epitope spans the β1 sheet outside the PDZ domain (Supplementary Fig. 2A bottom panels). This region of TIP-1 has not been reported to be involved in any protein-protein interactions. In the current study, Ab2 is designated as a non-PDZ/TIP1 antibody.

After finding the epitopes, we treated NSCLC and GB cells with either

anti-PDZ/TIP1 antibody, anti-non PDZ/TIP1 antibody, or isotype control (Fig. 3A). The anti-PDZ/TIP1 antibody significantly reduced proliferation ($p < 0.001$) of A549, LLC, D54, and GL261 cells when compared to the anti-non PDZ/TIP1 antibody or the isotype control (Fig. 3A). Since we observed a biological effect by targeting TIP1 with the Anti-PDZ/TIP1 antibody, we used this for all further experiments.

We found that the anti-TIP1 Ab did not affect the proliferation of healthy lung (MRC-5) and endothelial (HUVEC) cells, which is indicative of cancer specificity (Fig. 3B). Targeting TIP1 with the anti-TIP1 Ab reduced cell proliferation in a time-dependent manner in all cancer cell lines (Fig. 3C). Taking the proliferation at 0 h as 100 %, the percentage of proliferation for the isotype vs. anti-PDZ Ab treatment at 96 h was 3400 % vs 1946.6 % in A549 ($P < 0.0001$), 6666.67 % vs 3866.667 in H460 ($P < 0.0001$), 1133.33 % vs 446.67 % in D54 ($P < 0.0001$), and 1833.3 % vs 1100 % in U251 ($P < 0.0001$) respectively. (Fig. 3C).

To study the specificity of the anti-TIP1 Ab, we knocked out (KO) TIP1 using CRISPR/Cas9 in A549 and U251 cells. Protein analysis of A549 and U251 using western immunoblots showed a complete knockout of TIP1 (Fig. 3D). The whole western blot image used to generate Fig. 3D is shown in Supplementary Fig. 4I. The TIP1 KO A549 and U251 cells showed significantly reduced proliferation in a time-dependent manner when compared to A549 and U251 cells transduced with the CRISPR control (Fig. 3E). We then treated the TIP1 KO A549 and U251 cells with the anti-TIP1 Ab. The addition of the anti-TIP1 Ab to TIP1 knockout A549 and U251 cells did not further reduce proliferation. However, A549 and U251 cells with (CRISPR control) showed a significant reduction ($p < 0.001$) in proliferation after treatment with anti-TIP1 Ab (Fig. 3F). These results validate the target specificity of the anti-TIP1 Ab on cancer cells.

3.4. The anti-TIP1 antibody binds to PDZ pocket of TIP1 protein with high affinity

The affinity of the anti-TIP1 Ab to purified TIP1 protein was calculated using the BIAcore T200 system and found to be 0.12×10^{-9} M (Supplementary Fig. 2B). Anti-TIP1 antibody and TIP1 protein form a complex in vitro that was purified by using the S200 superdex 16/300GL gel filtration column, and a shift was observed compared to the anti-TIP1 antibody alone (Supplementary Fig. 2 C). The gel-filtered anti-TIP1 antibody in complex with the TIP1 protein was resolved on SDS-PAGE, and western blotting was performed to characterize the complex (Supplementary Fig. 2D). We further evaluated the gel-filtered anti-TIP1 Ab in complex with TIP1 protein by visualization of negative stain transmission electron microscopy (TEM) (Supplementary Fig. 2E). 2D class averaging and data analysis revealed two different orientations of the Ag-Ab complexes. A Linear complex, where two antigens are bound to the two Fab arms of the antibody, and a diamond complex, where two antigens are bound between two antibodies. To evaluate anti-TIP1 antibody targeting both human and mouse tumors, we aligned the amino acid sequence of the TIP1 protein from these two species using the Clustal Omega tool available on the Uniprot website. The Uniprot IDs for mouse and human TIP1 are Q9DBG9 and O14907 respectively. The alignment indicated 99.19% identity in the human and mouse TIP1 proteins (Supplementary Fig. 2F). The difference in the two proteins lies in the fourth position amino acid position, where "I" of the human TIP1 is replaced by "T" in the mouse TIP1 protein (Supplementary Fig. 2F). The epitope of the anti-TIP1 antibody lies outside the region of dissimilarity.

3.5. TIP1 blockade inhibits cell viability signaling

To identify potential mechanisms of antibody cytotoxicity, we performed RNA-sequencing at various times following Ab treatment (Fig. 4). Fig. 4A shows a Venn diagram representing the number of differentially expressed genes in the treatment groups. At 36 h after treatment, we found 3481 differentially expressed transcripts compared to the control. Volcano plots showing the distribution of genes in terms of –log10 p values on y-axis and log2 fold change on the x-axis for various groups are shown in Fig. 4B. Further, gene ontology (GO) analysis was performed for all treatment groups. GO analysis of cells treated with the anti-PDZ/TIP1 Ab revealed that the top 10 down-regulated GO biological processes included ribosome biogenesis, mitotic division, DNA replication, and cell cycle phase transition (Fig. 4C). The top 10 significantly upregulated GO processes are shown in Fig. 4D and include dephosphorylation, endocytosis, and apoptosis.

Since the AKT/mTOR pathway plays a significant role in cell proliferation, transcription, translation, and survival [29–31], we investigated this pathway following treatment with the anti-PDZ/TIP1 antibody. We observed reduced abundance of phospho-AKT, total AKT, phospho-4EBP1, phosphorylated and total levels of mTOR, in cells treated with anti-PDZ/TIP1 antibody (Fig. 5A). Whole western blot images that contributed to the generation of Fig. 5A are shown in Supplementary Fig. 4 (A-H).

3.6. The anti-TIP1 antibody internalizes and induces cell death by apoptosis in cancer cells

Antibody-mediated tumor cell killing has been found to involve antibody internalization [32]. Cetuximab (chimeric IgG1) and Necitumumab (human IgG1) are antibodies that target the epidermal growth factor receptor (EGFR) and are internalized [33]. Antibody-drug conjugates deliver drugs to cancer cells following endocytosis [34]. We evaluated anti-PDZ Ab for internalization speculating that signal transduction inhibition by anti-PDZ Ab may follow Ab internalization. We found endocytosis of the antibody within the cells as early as 2 h and saturated at 9–12 h (Fig. 5B).

We performed Annexin-V/PI staining to evaluate cell death in GB and NCSLC cells after anti-PDZ/TIP1 antibody treatment. Percentages of cells that have undergone late apoptosis (Annexin-V positive, PI positive) or dead (only PI-positive) are shown in Fig. 5C. We found that anti-PDZ/TIP1 antibody-induced apoptosis in A549 (3.5 %, $P < 0.05$), H460 (37.3 %, $P < 0.0001$), U251 (3.5 %) and D54 (10.5 %, $P < 0.0001$) cells (Fig. 5C). The percentage of dead cells following treatment with the anti-PDZ/TIP1 antibody was A549 (4.6 %, $P = 0.28$), H460 (38.3 %, $P < 0.0001$), U251 (20.7 %, $P < 0.0001$) and D54 (6.7 %, $P < 0.0001$).

Since TIP1 has been found to interact with FAS [35], we speculated the involvement of FAS receptor signaling in inducing cancer cell apoptosis following anti-PDZ Ab treatment. We performed quantitative mass spectrometry followed by *in silico* analysis using Ingenuity Pathway Analysis (IPA) software. We found activation of FAS receptor signaling, as shown in an IPA plot in Fig. 5D. The list of proteins and their experimental fold change identified by quantitative mass spectrometry is shown in the Supplementary table. To validate the involvement of the FAS receptor in anti-PDZ Ab-mediated cytotoxicity, we knocked down FAS using three different shRNAs (Fig. 5E). We found abrogation of the cytotoxic effects of the anti-PDZ Ab following FAS knockdown. Thus, the anti-PDZ Ab cell death signaling might involve the FAS death receptor, and TIP1 may be blocking cell death signaling through its interaction with FAS [35]. However, the anti-TIP1/PDZ antibody did not increase the percentage of apoptotic cells induced by treatment with Fas ligand (Supplementary fig. 3A).

3.7. TIP1 blockade delays tumor growth and enhances the cytotoxicity of radiation in mouse xenograft models

Radiation, in combination with chemotherapy, is the standard of care for GB and NSCLC [36,37]. We evaluated the efficacy of combining the anti-PDZ/TIP1 antibody with radiation using proliferation (Fig. 6A) and colony formation assays (Fig. 6B). We found that combining anti-PDZ antibodies with radiation reduced proliferation in A549 (25 %, $P < 0.05$), H460 (18 %, $P < 0.05$), U251 (42 %, $P < 0.05$), and D54 cells (30 %) when compared to either anti-PDZ antibody alone or isotype

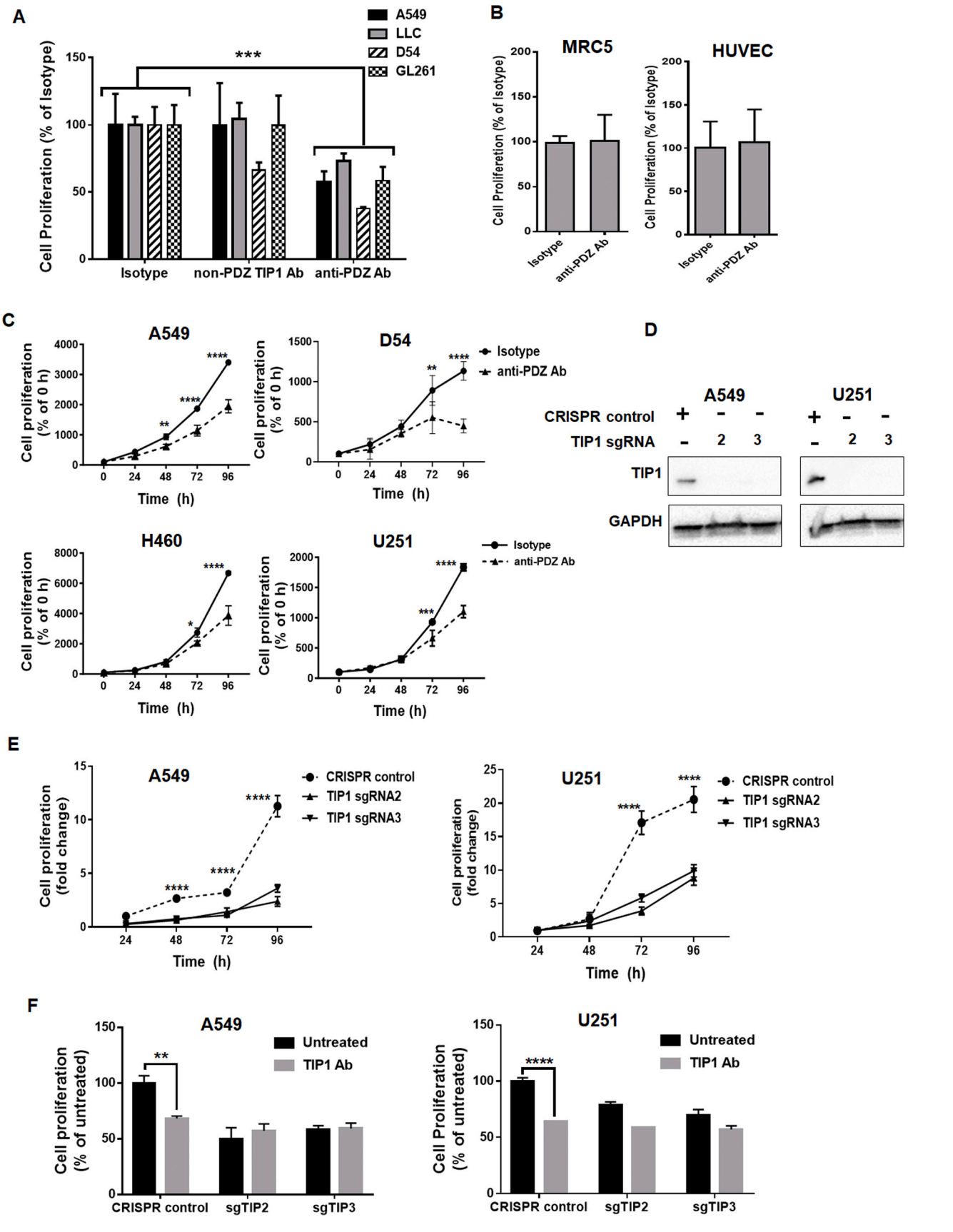

(caption on next page)

Fig. 3. Antibodies targeting the functional PDZ domain of TIP1 inhibit NSCLC and GB proliferation in vitro. (A) NSCLC (A549 and LLC) and GB (D54 and GL261) cell proliferation at 96 h following treatment with anti-PDZ/TIP1 antibody is compared to non-PDZ/TIP1 antibody. Proliferating cells were evaluated using Trypan blue dye exclusion assays. Shown are the mean percentages of proliferating cells relative to the isotype control and SD from three treatments. * ** $P < 0.001$. (B) Anti-PDZ/TIP1 Ab treatment does not alter cell viability in normal lung (MRC-5) and endothelial (HUVEC) cells. Cells were treated with 1 μg/ml anti-PDZ/TIP1 or isotype control antibody for 96 h. Trypan blue dye exclusion assay was performed to count the viable cells. Shown are the percent viable cells as a bar graph with SD from three treatments. (C) Anti-PDZ/TIP1 Ab treatment reduces the proliferation of NSCLC and GB cells in a time-dependent manner. A549, H460, D54, and U251 cells were treated with 1 μg/ml of the anti-PDZ/TIP1 antibody or isotype control antibody for 24 h, 48 h, 72 h, and 96 h. Proliferating cells were evaluated by trypan blue dye exclusion assay at the indicated time points. Shown are the percentages of proliferating cells relative to 0 h and SD from three different experiments * $P < 0.05$, * *$P < 0.01$, * ** $P < 0.001$, * ** * $P < 0.0001$. (D) To evaluate the knockout of TIP1, A549 and U251 cells were transduced with two TIP1 sgRNA (2 and 3) and a control vector. Protein extracts of transduced cells were blotted and probed using antibodies against TIP1. Protein loading was evaluated using GAPDH (Cell Signaling Technology). (E) The proliferation of A549 and U251 cells, which were transduced with either CRISPR control vector or TIP1 sgRNAs, was evaluated by the trypan blue dye exclusion assay at the indicated time points. Shown are the mean fold change in cell number relative to CRISPR control and SD from three different experiments. (F) TIP1 knockout abrogates the effect of the anti-PDZ/TIP1 antibody on cell proliferation. A549 and U251 cells having TIP1 KO were treated with anti-PDZ/TIP1 antibody, and cell proliferation was evaluated. Shown are the mean percentages of proliferating cells relative to the untreated CRISPR control cells and SD from three treatments. * $P < 0.05$, * ** $P < 0.001$, * ** * $P < 0.0001$.

with radiation (Fig. 6A). Using colony formation assays, we found that treatment with anti-PDZ/TIP1 antibody attenuated the surviving fraction in A549, H460, U251, and D54 cells in combination with radiation (Fig. 6B). We calculated the sensitivity enhancement ratios at 3 Gy ($SER_{3\ Gy}$), 5 Gy ($SER_{5\ Gy}$), and 7 Gy ($SER_{7\ Gy}$) compared to the isotype control. The $SER_{3\ Gy}$ for A549, H460, U251 and D54 cells were 1.16 ± 0.13, 1.14 ± 0.08, 1.13 ± 0.03, and 1.08 ± 0.08 respectively. The $SER_{5\ Gy}$ for A549, H460, U251 and D54 cells were 2.07 ± 0.15 ($P < 0.0001$), 1.37 ± 0.45 ($P = 0.03$), 1.26 ± 0.32 ($P = 0.25$), and 2.26 ± 0.82 ($P = 0.04$) respectively (Fig. 6B). The $SER7_{Gy}$ for A549, H460, U251 and D54 cells were 1.72 ± 0.15 ($P < 0.0001$), 2.05 ± 0.31 ($P < 0.0001$), 2.94 ± 0.27 ($P < 0.0001$), 2.0 ± 0.0 ($P = 0.51$) respectively.

The in vivo therapeutic efficacy of the anti-PDZ/TIP1 antibody was determined in nude mice bearing heterotopic human NSCLC (A549) and glioblastoma (U251) tumors (Fig. 6 C). Subtherapeutic doses of antibodies and radiation were administered to determine whether interactive cytotoxicity was achieved. In both the tumor models, we compared the following groups: isotype control antibody alone, isotype control in combination with radiation (XRT) (five fractions of 2 Gy), anti-PDZ/TIP1 antibody (two doses of 300 μg antibody) alone or with radiation (five fractions of 2 Gy. Mice treated with anti-PDZ/TIP1 antibody in combination with radiation had significantly smaller tumors after the study than isotype control in combination with radiation in both A549 and U251. Mice treated with isotype control antibody developed maximum allowable tumor volume within 30–35 days in both models (Fig. 6C). In contrast, tumors in mice treated with anti-PDZ/TIP1 antibody in combination with radiation were only 1272 mm^3 for A549 and 788 mm^3 for U251 after the study (Fig. 6C). We determined the survival of mice in each of the treatment groups. Fig. 6D shows the Kaplan-Meier survival curves for mice bearing A549 and U251 tumors. Anti-PDZ Ab alone significantly increases the survival of tumor-bearing mice as compared to the Isotype control antibody ($P < 0.01$) (Fig. 6D). When administered during radiotherapy, the anti-PDZ antibody further enhances the survival of mice bearing A549 or U251 tumors ($P < 0.01$) (Fig. 6D).

Furthermore, mice in all groups had weight gain during the study and did not show physical features that would suggest systemic toxicity from the antibody (Supplementary Fig. 3B).

4. Discussion

TIP1 plays a role in cancer cell adhesion, migration, and metastasis [16–18]. TIP1 binding proteins include enzymes participating in cell viability signaling pathways like PLC, PKC, GPCR, and Rho [6, 13, 38–40]. Through these protein interactions, TIP1 demonstrates versatility in biological functions, such as mediating the cellular response to serum starvation [39], inhibiting beta-catenin, regulating gene transcription and cell proliferation [13], establishing polarity of cells [38], and protecting tumor cells from ionizing radiation-induced cell death [7, 18]. TIP1 is overexpressed in many cancers, and its levels correlate with tumor progression and poor prognosis [6,7]. We analyzed the TCGA lung cancer and glioblastoma dataset and found correlations between high TIP1 expression levels with worsened overall survival of patients. In human lung cancer tumor tissue microarray having matched healthy lung tissues, we found increased expression of TIP1 in tumors, compared to the matched healthy tissues. No expression of TIP1 was observed in healthy tissue microarrays. We also found overexpression of TIP1 in heterotopic mouse models of cancer. For all experiments in this study, we chose a fractionated radiation scheme based on our prior publications [7,9,12,18] and to replicate patient dosing. Using NIR imaging, we found significantly upregulated TIP1 expression in A549 and U251 tumors in nude mice, which was further enhanced by radiation. Microscopic bio-distribution of the tumor sections also supported enhanced extravasation of the anti-TIP1 antibody in tumors following irradiation. In contrast, radiation treatment did not induce TIP1 on the surface of normal lung fibroblasts MRC5.

TIP1 comprises a single type I PDZ domain, which selectively recognizes the C-terminal S/T-X-V/L-COOH motif of its interacting partners [12, 26–28]. TIP1 consists of six-stranded antiparallel β-sheets flanked by two α-helices. The crystal structure of TIP1 with its ligand shows that the ligand binds PDZ in a groove lying between the β2-strand and α2-helix [11]. The ILGF motif is a crucial structural binding motif in this groove. The COOH group of the incoming ligand forms a hydrogen bond with the glycine (G) of this ILGF motif. Isoleucine (I), leucine (L), and phenylalanine (F) contribute hydrophobicity to the binding pocket. This hydrophobicity leads to the entry of the TIP1 ligand into the functional PDZ domain and the stabilization of the interaction. The ILGF motif is not found in the PDZ domains of other proteins and is unique to the TIP1 PDZ domain. Thus, the effects of the treatment with the anti-PDZ antibody are specific to TIP1. The TIP1 PDZ also contains a hairpin loop composed of antiparallel β-strands (βa and βb), which is absent in PDZ domains of other proteins [11]. Structural analysis of the location of the epitopes to the anti-PDZ/TIP1 antibody revealed that they spanned the entire hairpin loop, ILGF motif, and the β2-strand of the PDZ binding groove, all of which are important for binding to TIP1 ligands. We evaluated the cytotoxic effects of anti-TIP1 antibodies in treating GB and NSCLC cells. We selected two TIP1 antibodies, one cytotoxic and another not cytotoxic to GB and NSCLC cells. The epitope of the cytotoxic antibody mapped in the functional PDZ domain of TIP1, while the epitope of the antibody that was not cytotoxic mapped outside the PDZ domain. We designated the antibody bound within the active PDZ domain as anti-PDZ/TIP1 antibody. This analysis suggests that the binding of the anti-PDZ/TIP1 antibody might interfere with the interaction of TIP1 with its protein partners by blocking its functional domain. In contrast, the non-PDZ antibody [12], which binds close to the N-terminal β1 of TIP1, outside of the PDZ domain, is not expected to prevent the interaction of TIP1 with other proteins. We earlier described the non-PDZ antibody for targeting cancers by conjugating it to a radioisotope yttrium-90 (^{90}Y) [12]. The tumor inhibitory effects of the

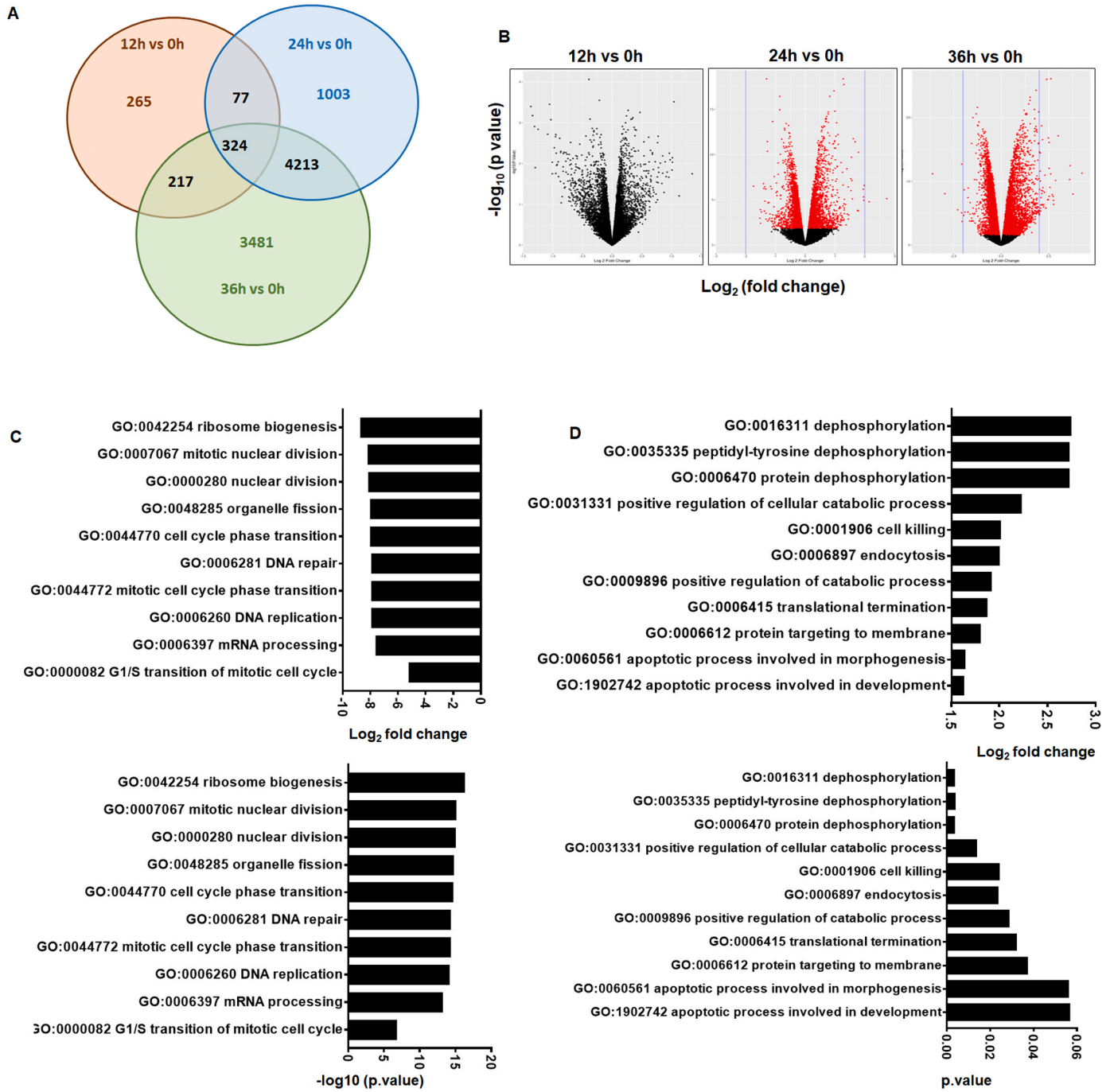

Fig. 4. Transcriptomic analysis of blocking TIP1 functions reveals alterations in cell signaling pathways. (A) RNA-Seq analysis was performed to identify potential mechanisms of cytotoxicity of the anti-PDZ Ab. Venn diagram indicating the numbers of unique or shared genes expressed across contrasts that are significantly differentially expressed with Benjamini-Hochberg FDR adjusted p-values ≤ 0.05 and in combination with an observed log2 fold-change $\geq$ absolute value of 2. The number of genes annotated is listed in each diagram component. (B) Volcano plot showing the distribution of -log10 (p-value) vs. log2 (Fold Change). The horizontal axis represents the log2 (Fold Change) between the samples indicated while the vertical axis represents the -log10(p-value) for the differential expressions between the samples. Each point represents a gene; red points indicate p-value ≤ 0.05, while blue points indicate that p-value > 0.05. (C) Bar graph showing mean log2 fold change of the top 10 Gene Ontology (GO) biological processes downregulated 36 h after treatment with the anti-PDZ Ab (top). The bottom panel shows –log10 p-values of the same top 10 GO biological processes shown in the top panel. (D) Bar graph showing mean log2 fold change of the top 10 Gene Ontology (GO) biological processes upregulated 36 h after treatment with the anti-PDZ Ab (top). The bottom panel shows p-values of the same top 10 GO biological processes shown in the top panel.

non-PDZ antibody in our previous study are attributed to the β- emitter ^{90}Y conjugated to this antibody [12]. In line with our current study, the naked non-PDZ antibody did not delay the growth of tumors in vivo [12]. These observations further display the importance of blocking the functional ligand-binding domain of TIP1 for direct cytotoxic effects.

The anti-PDZ/TIP1 antibody was tightly bound to the TIP1 protein in vitro and purified as an antigen-antibody complex by gel filtration. The affinity of the anti-PDZ/TIP1 Ab (0.12×10^{-9} M) also confirmed tight binding. Negative stain transmission electron microscopy and 2D class averaging revealed a linear and diamond-shaped antigen-antibody

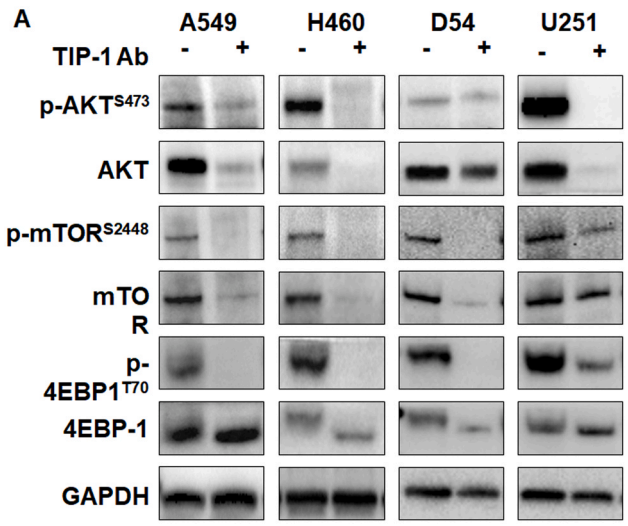

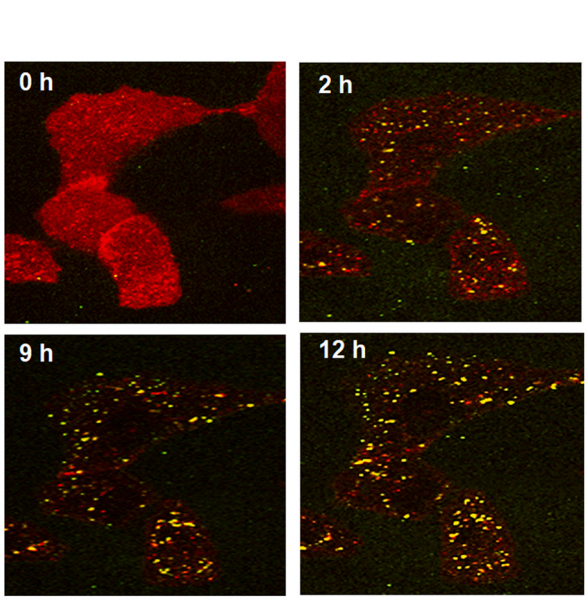

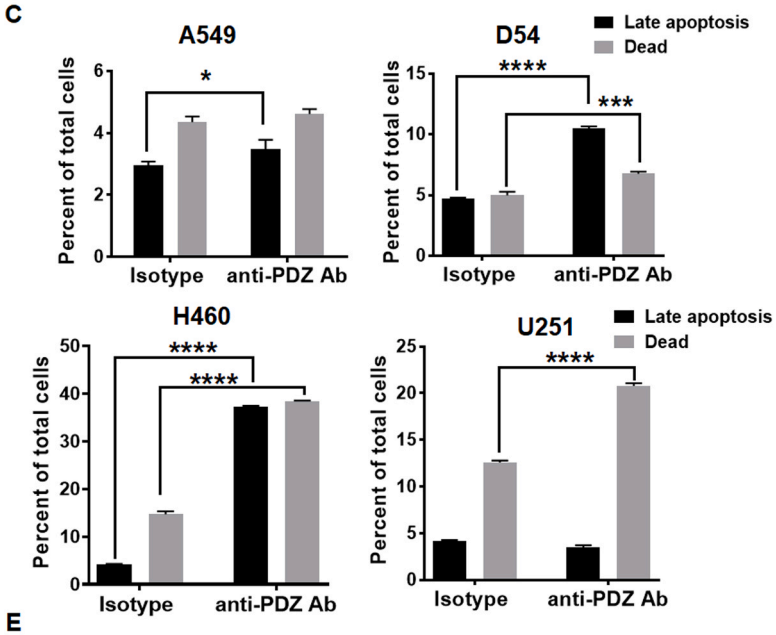

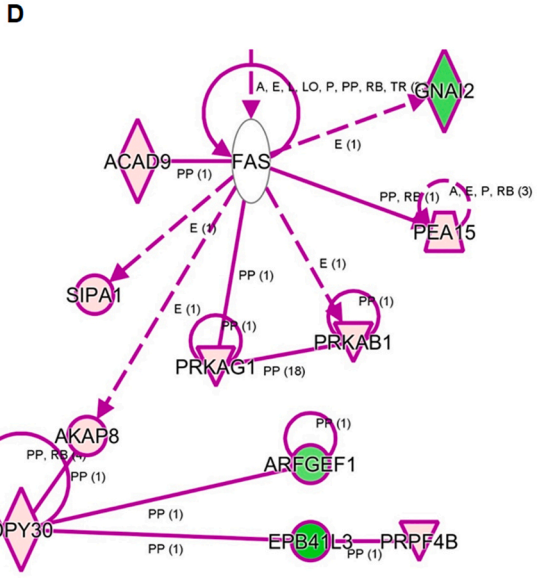

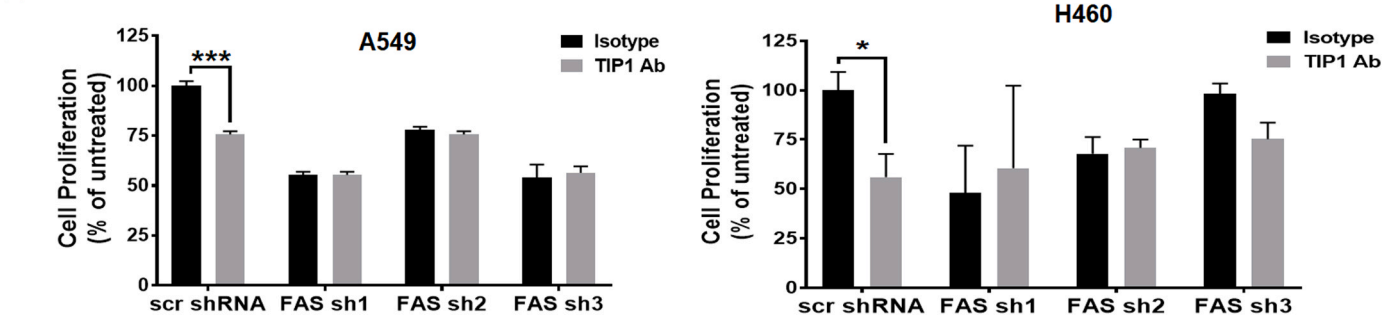

(caption on next page)

Fig. 5. TIP1 blockade downregulates AKT/mTOR signaling and induces cell death by apoptosis (A) Treatment with the anti-PDZ/TIP1 antibody downregulates AKT and mTOR signaling in NSCLC and GB cell lines. Lung cancer (A549 and H460) and glioblastoma (D54 and U251) cells were treated with 1 μg/ml of anti-PDZ/TIP1 antibody for 96 h. Total cellular protein was immunoblotted using antibodies against phospho-AKT (S473), total AKT, phospho-mTOR (S2448), total mTOR, phospo-4EBP1 (T70), 4EBP1 (T70) with GAPDH as a loading control. (B) Live-cell fluorescent imaging illustrating the internalization of anti-PDZ/TIP1 antibody. A549 cells were labeled with Cell mask orange dye 24 h after seeding. Immediately after labeling, cells were treated with Alexa-Flour 488 labeled anti-PDZ/TIP1 antibody. Live cell Z stack images were captured every 5 min using a spinning-disk confocal microscope (Nikon Eclipse Ti-E). Shown are representative images at the various indicated time points. Red: cell mask orange labeled cells, Green: Alexa-Flour 488 labeled anti-PDZ/TIP1 antibody and Yellow: Internalized anti-PDZ/TIP1 antibody. (C) Annexin V/PI assays with lung cancer (A549 and H460) and glioblastoma (D54 and U251) cells. A549, H460, D54, and U251 cells were treated with 1 μg/ml of anti-PDZ/TIP1 antibody. Cells were stained with Annexin V and PI 96 h after treatment and analyzed by flow cytometry. Shown are the mean percentages of late apoptotic cells (Annexin V and PI positive) and dead cells (PI-positive) with SD from three different experiments * $P < 0.05$, * ** $P < 0.001$, * ** * $P < 0.0001$. (D) The FAS pathway is activated following anti-PDZ/TIP1 antibody treatment. Quantitative proteomics was performed following anti-PDZ/TIP1 antibody treatment. Data were analyzed using the ingenuity pathway analysis and shown is a representative pathway map indicating activation of the FAS pathway. (E) The knockdown of FAS abrogates the cytotoxic effects of the anti-PDZ/TIP1 antibody. A549 cells were treated with five different shRNAs against FAS or scrambled (scr) shRNA. Following knockdown of FAS, cells were treated with 1 μg/ml of anti-PDZ/TIP1 antibody, and cell proliferation was evaluated. Shown are the mean percentages of proliferating cells relative to the isotype treated scr cells and SD from three treatments. * $P < 0.05$, * ** $P < 0.001$, * ** * $P < 0.0001$.

complex. We found 99.19% identity in the human and mouse TIP1. The epitope of the anti-PDZ/TIP1 antibody lies in the region of similarity allowing this antibody to target both human and mouse tumors. The high degree of similarity in the human and mouse TIP1 makes the mouse a suitable host for predicting potential toxicity from non-desirable binding to normal human tissues.

The treatment of GB and NSCLC cells with the anti-PDZ/TIP1 antibody inhibited proliferation. In contrast, treating normal cells with anti-PDZ/TIP1 antibodies did not alter their proliferation. Thus, this biological activity of the anti-PDZ/TIP1 antibody appears specific to cancer cells due to the overexpression of TIP1 in cancer cells. We observed a similar inhibition in proliferation when we knocked out TIP1 from A549 and U251 cells using the CRISPR/Cas9 technology. The target specificity of the anti-PDZ/TIP1 antibody was confirmed by treating the TIP1 knockout cells with the antibody. Knocking out TIP1 abrogated the cytotoxic effect of the anti-PDZ/TIP1 on these cells.

Antibody internalization has been shown to contribute to cancer cell killing by other therapeutic antibodies [32], such as Cetuximab (chimeric IgG1), Necitumumab (human IgG1) which are internalized after binding to epidermal growth factor receptor (EGFR) [33]. We observed internalization of the anti-PDZ/TIP1 antibody within 2 h after treatment, and it peaks at 12 h post-treatment. This internalization process is temporally followed by perturbations in the cellular functions of TIP1, resulting in cytotoxicity. The internalization of antibodies has been shown to induce apoptosis in cancer cells. Antibodies like cetuximab that target EGFR, Rituximab, Tositumomab that target CD20, and CAMPATH-1 H that target CD52 all induce cell death by apoptosis [41]. We observed that GB and NCSLC cells also undergo cell death by apoptosis after anti-PDZ/TIP1 antibody treatment but there may be additional mechanisms of cell death involved. Since TIP1 interacts with FAS [35], we speculated the involvement of FAS receptor signaling. Using quantitative mass spectrometry, we found activation of FAS receptor signaling. We knocked down FAS in A549 and H460 cells to study this further. Interestingly, we observed a slight reduction in the proliferation of cells treated with FAS shRNAs. This may be attributed to the growth-promoting effects of FAS, as described earlier [42,43]. However, no further reduction in cell proliferation by the anti-PDZ/TIP1 antibody was observed in the FAS shRNA-treated cells. This suggests that TIP1 may be blocking downstream signaling through FAS [35] and that the anti-PDZ/TIP1 antibody unleashes this cell death signaling by blocking TIP1-FAS interaction. However, the anti-TIP1/PDZ antibody did not increase the percentage of apoptotic cells induced by treatment with Fas ligand. The role of FAS on anti-PDZ Ab-induced apoptosis needs further investigation.

To identify potential mechanisms of antibody cytotoxicity, we performed RNA Sequencing following antibody treatment. Several differentially expressed transcripts were observed compared to the controls. Gene Ontology and KEGG analysis revealed that the top significantly downregulated processes included ribosome biogenesis, mitotic division, and cell cycle phase transition. Since the AKT and mTOR pathways are essential regulators of cell proliferation, metabolism, and survival, we investigated this pathway following anti-PDZ/Ab treatment. We observed the downregulation of AKT and mTOR signaling following treatment with the anti-PDZ/TIP1 antibody. Earlier, we reported that TIP1 is essential for activating Rho GTPases (RhoA, Cdc42, and Rac1) during migration in GB cells [44]. AKT is downstream of Rac1, and its phosphorylation by Rac1 may be a feedback regulation mechanism [45]. Since the TIP1 knockdown decreased Rac1 activity [35], we speculate that the anti-PDZ/TIP1 antibody could downregulate the AKT/mTOR pathway through Rac1 activity. PDZ domain-containing proteins are known to assist in organizing protein complexes [46,47]. TIP1 may also play a role in assembling the mTOR signaling protein complexes.

External beam radiotherapy (XRT) is a commonly used therapeutic modality for GB and NSCLC. Analysis of microarray datasets from GB patients revealed that elevated TIP1 correlates with a poor prognosis of human malignant gliomas after radiotherapy [18]. Treatment with anti-PDZ/TIP1 antibody alone resulted in a significant reduction of proliferation, and in combination with radiation (3 Gy), led to an enhanced cytotoxic effect. Treatment of H460 cells with the anti-PDZ/TIP1 antibody led to higher cytotoxicity than in the other cell lines; a combination antibody with radiation did not lead to further cytotoxicity. The reason for less additive killing is not apparent, but antibody treatment showed further enhancement of radiation cytotoxicity in the colony formation assay.

We have previously demonstrated activation of the mouse immune effector cells by 2C6F3 which is a mouse anti-TIP1 antibody [12]. Syngeneic mouse models were not used in this study since we don't expect the anti-PDZ/TIP1 antibody raised in goat to activate the mouse immune effector cells. Here, we studied the effect of blocking TIP1 on tumor growth in human cancer xenograft models. Treatment with anti-PDZ/TIP1 antibody alone led to tumor growth delay in heterotopic tumor models of GB and NSCLC. Two administrations with anti-PDZ/TIP1 antibodies were sufficient to significantly delay tumor growth and improve the survival of both GB and NSCLC mouse models. We did not find tumor retention of the isotype control antibody in NIR imaging studies and therefore compared the anti-PDZ antibody treatment in combination with radiation to the isotype control in combination with radiation. The anti-PDZ antibody treatment enhanced the efficacy of radiation as compared to the isotype control in combination with radiation. As a measure of potential toxicity, we did not find a reduction in mouse body weights after treatment or any other visual signs of distress. The tumor growth delay could be due to the blocking of survival pathways, such as AKT and mTOR, which are required for cancer cell proliferation. The mechanism of this downregulation by the anti-PDZ/TIP1 antibody is a subject of future studies. Combining anti-PDZ/TIP1 antibody treatment with radiation had an additive effect, indicating that radiation does not interfere with the cytotoxic effects of the anti-PDZ/TIP1 antibody. The anti-PDZ/TIP1 antibody could be combined with radiation to increase the effectiveness of XRT in NSCLC and GB patients.

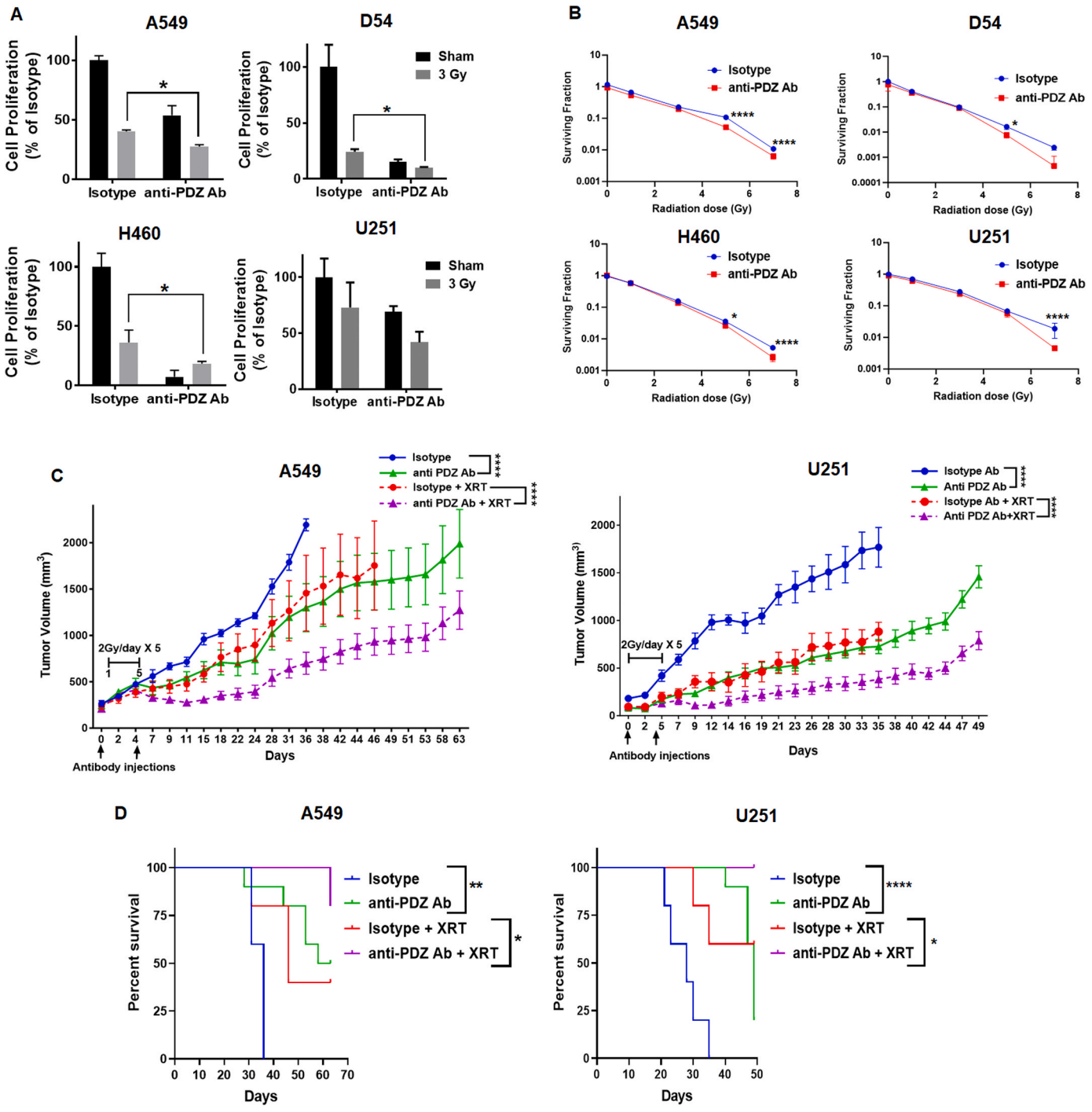

Fig. 6. TIP1 blockade enhances the efficacy of radiation therapy in vitro and in vivo. Treatment with anti-PDZ/TIP1 antibody delays the growth of A549 and U251 tumor xenografts. (A) Treatment with anti-PDZ/TIP1 antibody enhances the cytotoxicity of radiation. Lung cancer (A549 and H460) and glioblastoma (D54 and U251) cells were treated with 1 μg/ml antibody and irradiated with 3 Gy or 0 Gy. Trypan blue dye exclusion assay was performed after 96 h. Shown are the percent viable cells as a bar graph with SD from three treatments. (B) Colony formation assay was performed on A549, H460, D54, and U251 cells treated with 1 μg/ml of anti-PDZ/TIP1 antibody or isotype control Ab for 96 h. Cells were then irradiated with 1, 3, 5, and 7 Gy and incubated for 10–14 days. Colonies comprising of 50 or more cells were scored. Shown are the mean surviving fraction normalized to the isotype control with SD from three different experiments. * $P < 0.05$, * ** * $P < 0.0001$. (C) A549 and U251 cells were implanted bilaterally into the hindlimbs of athymic nude mice. Once the tumors were palpable (~200mm3), the tumors on the right flank were irradiated with 2 Gy for five consecutive days. The tumors on the left flank served as sham controls. The tumor-bearing mice were treated with anti-PDZ/TIP1 antibody or isotype control antibody on days 1 and 4 after radiation. Tumor volumes were measured using digital calipers. Displayed is the line graph of the mean tumor volumes ± s.e.m. for A549 and U251. (D) Shown are the Kaplan- Meier survival curves of nude mice bearing A549 or U251 tumors treated with anti-TIP1 antibody in combination with radiation or the control groups. Statistical analysis for survival curves was performed using the Log-rank (Mantel-Cox) test. * , $P < 0.05$; * *, $P < 0.01$; * ** , $P < 0.001$, * ** *$P < 0.0001$.

In conclusion, this study suggests that radiation-inducible TIP1 is a potential molecular target for the therapy of NSCLC and GB. Blocking the functional PDZ domain with a specific antibody is a new strategy for targeted therapy for NSCLC and GB, especially in combination with radiotherapy. Not only can we block the function of TIP1, we can also use this target to deliver payloads to tumors that are treated with radiation. We are developing human antibodies against TIP1 that will be studied in clinical trials as an investigational new drug. Our goal is to use the radiolabeled human antibodies for non-invasive positron-emission tomography (PET) imaging for patient stratification to optimize therapeutic efficacy in TIP1-positive tumors.

Funding

This study was supported by NCI grants to Dennis Hallahan R41 CA192413, R21CA170169, Institutional Clinical, and Translational Science U54RR024992 and the Foundation for Barnes Jewish Hospital and the Lung Cancer Research Foundation (Vaishali Kapoor), K22CA234404 (Vaishali Kapoor).

CRediT authorship contribution statement

Abhay K. Singh: Methodology, Software, Validation, Formal analysis, Investigation, Writing- Original Draft. **David YA Dadey**: Methodology, Investigation, Writing- Original Draft. **Michael J. Rau:** Investigation, Software. **James Fitzpatrick**: Methodology, Writing - Review & Editing. **Harendra K. Shah**: Investigation, Formal analysis. **Minakshi Saikia**: Investigation, Formal analysis. **Reid Townsend**: Methodology, Software. **Dinesh Thotala**: Formal analysis, Writing - Review & Editing. **Dennis E. Hallahan**: Conceptualization, Methodology, Resources, Writing- Review & Editing, Supervision, Funding acquisition. **Vaishali Kapoor**: Conceptualization, Methodology, Software, Validation, Formal analysis, Investigation, Resources, Writing- Original Draft, Writing - Review & Editing, Supervision, Funding acquisition.

Declaration of Competing Interest

Dr. Hallahan is a founder and shareholder of Medical Guidance Systems LLC, which is developing human anti-TIP1 antibodies. Vaishali Kapoor, and Abhay Kumar Singh are inventors on pending patents. Other authors state that there are no conflicts of interest. All authors agree to send an individual conflict of interest form if requested by the journal.

Acknowledgments

We thank research technicians Arpine Khudanyan, Anrea Collins and Kelly Hoye for assistance in the experiments. We thank Amanda Klass for tail vein injections. We thank Dennis Oakley at the Washington University Center for Cellular Imaging for assistance in confocal microscopy and Petra Gilmore at the Washington University Proteomics core for quantitative proteomics analysis. We also thank the Siteman Cancer Center shared research facilities and the Elizabeth &James McDonnell Endowment for DH.

Appendix A. Supporting information

Supplementary data associated with this article can be found in the online version at doi:10.1016/j.biopha.2023.115341.

References

[1] R. Rosell, N. Karachaliou, Lung cancer: maintenance therapy and precision medicine in NSCLC, Nat. Rev. Clin. Oncol. 10 (10) (2013) 549–550.
[2] P.D. Delgado-Lopez, E.M. Corrales-Garcia, Survival in glioblastoma: a review on the impact of treatment modalities, Clin. Transl. Oncol.: Off. Publ. Fed. Span. Oncol. Soc. Natl. Cancer Inst. Mex. 18 (11) (2016) 1062–1071.
[3] E.A. Donovan, S. Kummar, Targeting VEGF in cancer therapy, Curr. Probl. Cancer 30 (1) (2006) 7–32.
[4] Y. Zhang, F. Guessous, A. Kofman, D. Schiff, R. Abounader, XL-184, a MET, VEGFR-2 and RET kinase inhibitor for the treatment of thyroid cancer, glioblastoma multiforme and NSCLC, Idrugs 13 (2) (2010) 112–121.
[5] A. Passaro, C. Lazzari, N. Karachaliou, G. Spitaleri, A. Pochesci, C. Catania, et al., Personalized treatment in advanced ALK-positive non-small cell lung cancer: from bench to clinical practice, OncoTargets Ther. 9 (2016) 6361–6376.
[6] H. Wang, M. Han, W. Whetsell, J. Wang, J. Rich, D. Hallahan, et al., Tax-interacting protein 1 coordinates the spatiotemporal activation of Rho GTPases and regulates the infiltrative growth of human glioblastoma, Oncogene 33 (12) (2014) 1558–1569.
[7] H. Wang, H. Yan, A. Fu, M. Han, D. Hallahan, Z. Han, TIP-1 translocation onto the cell plasma membrane is a molecular biomarker of tumor response to ionizing radiation, PLOS One 5 (8) (2010), e12051.
[8] G. Hariri, H. Yan, H. Wang, Z. Han, D.E. Hallahan, Radiation-guided drug delivery to mouse models of lung cancer, Clin. Cancer Res. 16 (20) (2010) 4968–4977.
[9] V. Kapoor, A.K. Singh, B. Rogers, D. Thotala, D.E. Hallahan, PEGylated peptide to TIP1 is a novel targeting agent that binds specifically to various cancers in vivo, J. Control Release (2019) (Accepted).
[10] B.Z. Harris, W.A. Lim, Mechanism and role of PDZ domains in signaling complex assembly, J. Cell Sci. 114 (Pt 18) (2001) 3219–3231.
[11] S. Mohanty, M. Ovee, M. Banerjee, PDZ domain recognition: insight from human tax-interacting protein 1 (TIP-1) interaction with target proteins, Biology 4 (1) (2015) 88–103.
[12] H. Yan, V. Kapoor, K. Nguyen, W.J. Akers, H. Li, J. Scott, et al., Anti-tax interacting protein-1 (TIP-1) monoclonal antibody targets human cancers, Oncotarget (2016).
[13] M. Kanamori, P. Sandy, R. Benetti, C. Kai, Y. Hayashizaki, The PDZ protein taxinteracting protein-1 inhibits beta-catenin transcriptional activity and growth of colorectal cancer cells, J. Biol. Chem. 278 (40) (2003) 38758–38764.
[14] B. Kay, J. Kehoe, PDZ domains and their ligands, Chem. Biol. 11 (2004) 423–425.
[15] D.L. Zoetewey, M. Ovee, M. Banerjee, R. Bhaskaran, S. Mohanty, Promiscuous binding at the crossroads of numerous cancer pathways: insight from the binding of glutaminase interacting protein with glutaminase L, Biochemistry 50 (17) (2011) 3528–3539.
[16] M. Han, H. Wang, H. Zhang, Z. Han, The PDZ protein TIP-1 facilitates cell migration and pulmonary metastasis of human invasive breast cancer cells in athymic mice, Biochem. Biophys. Res. Commun. 422 (1) (2012) 139–145.
[17] M. Han, Expression of Tax-interacting protein 1 (TIP-1) facilitates angiogenesis and tumor formation of human glioblastoma cells in nude mice, Cancer Lett. 328 (1) (2013) 55–64.
[18] M. Han, Expression of TIP-1 confers radioresistance of malignant glioma cells, PLOS One 7 (9) (2012), e45402.
[19] J. Zhang, X. Yan, C. Shi, X. Yang, Y. Guo, C. Tian, et al., Structural basis of beta-catenin recognition by Tax-interacting protein-1, J. Mol. Biol. 384 (1) (2008) 255–263.
[20] V. Kapoor, A.K. Singh, S. Dey, S.C. Sharma, S.N. Das, Circulating cycloxygenase-2 in patients with tobacco-related intraoral squamous cell carcinoma and evaluation of its peptide inhibitors as potential antitumor agent, J. Cancer Res. Clin. Oncol. 136 (12) (2010) 1795–1804.
[21] A.K. Singh, R. Singh, F. Naz, S.S. Chauhan, A. Dinda, A.A. Shukla, et al., Structure based design and synthesis of peptide inhibitor of human LOX-12: in vitro and in vivo analysis of a novel therapeutic agent for breast cancer, PLOS One 7 (2) (2012), e32521.
[22] V. Kapoor, D.Y. Dadey, K. Nguyen, S.A. Wildman, K. Hoye, A. Khudanyan, et al., Tumor-specific binding of radiolabeled PEGylated GIRLRG peptide: a novel agent for targeting cancers, J. Nucl. Med. 57 (12) (2016) 1991–1997.
[23] N.E. Sanjana, O. Shalem, F. Zhang, Improved vectors and genome-wide libraries for CRISPR screening, Nat. Methods 11 (8) (2014) 783–784.
[24] N.A. Franken, H.M. Rodermond, J. Stap, J. Haveman, C. van Bree, Clonogenic assay of cells in vitro, Nat. Protoc. 1 (5) (2006) 2315–2319.
[25] D.Y.A. Dadey, V. Kapoor, K. Hoye, A. Khudanyan, A. Collins, D. Thotala, et al., Antibody targeting GRP78 enhances the efficacy of radiation therapy in human glioblastoma and non-small cell lung cancer cell lines and tumor models, Clin. Cancer Res 23 (10) (2017) 2556–2564.
[26] Z. Tang, C. Li, B. Kang, G. Gao, C. Li, Z. Zhang, GEPIA: a web server for cancer and normal gene expression profiling and interactive analyses, Nucleic Acids Res. 45 (W1) (2017) W98–W102.
[27] Z. Han, A. Fu, H. Wang, R. Diaz, L. Geng, H. Onishko, et al., Noninvasive assessment of cancer response to therapy, Nat. Med. 14 (3) (2008) 343–349.
[28] V. Kapoor, A.K. Singh, C.D. Lewis, S. Deore, D.E. Hallahan, Exploiting radiation induction of antigens in cancer: targeted drug delivery, Int J. Mol. Sci. 23 (6) (2022).
[29] H.-F. Li, J.-S. Kim, T. Waldman, Radiation-induced Akt activation modulates radioresistance in human glioblastoma cells, Radiat. Oncol. 4 (2009) 43.
[30] Q.-W. Fan, W.A. Weiss, Targeting the RTK-PI3K-mTOR axis in malignant glioma: overcoming resistance, Curr. Top. Microbiol. Immunol. 347 (2010) 279–296.
[31] C. Mayer, I. Grummt, Ribosome biogenesis and cell growth: mTOR coordinates transcription by all three classes of nuclear RNA polymerases, Oncogene 25 (48) (2006) 6384–6391.
[32] A.M. Scott, J.D. Wolchok, L.J. Old, Antibody therapy of cancer, Nat. Rev. Cancer 12 (4) (2012) 278–287.

[33] M.B. Topper, J.R. Tonra, B. Pytowski, S.W. Eastman, Differentiation between the EGFR antibodies necitumumab, cetuximab, and panitumumab: antibody internalization and EGFR degradation, J. Clin. Oncol.: Off. J. Am. Soc. Clin. Oncol. 29 (15_suppl) (2011), e13022.
[34] C.D. Lewis, A.K. Singh, F.F. Hsu, D. Thotala, D.E. Hallahan, V. Kapoor, Targeting a radiosensitizing antibody-drug conjugate to a radiation-inducible antigen, Clin. Cancer Res. 27 (11) (2021) 3224–3233.
[35] M. Banerjee, C. Huang, J. Marquez, S. Mohanty, Probing the structure and function of human glutaminase-interacting protein: a possible target for drug design, Biochemistry 47 (35) (2008) 9208–9219.
[36] A. Auperin, C. Le Pechoux, E. Rolland, W.J. Curran, K. Furuse, P. Fournel, et al., Meta-analysis of concomitant versus sequential radiochemotherapy in locally advanced non-small-cell lung cancer, J. Clin. Oncol.: Off. J. Am. Soc. Clin. Oncol. 28 (13) (2010) 2181–2190.
[37] I.J. Barani, D.A. Larson, Radiation therapy of glioblastoma, Cancer Treat. Res. 163 (2015) 49–73.
[38] C. Alewine, O. Olsen, J.B. Wade, P.A. Welling, TIP-1 has PDZ scaffold antagonist activity, Mol. Biol. Cell 17 (10) (2006) 4200–4211.
[39] C. Reynaud, S. Fabre, P. Jalinot, The PDZ protein TIP-1 interacts with the Rho effector rhotekin and is involved in Rho signaling to the serum response element, J. Biol. Chem. 275 (43) (2000) 33962–33968.
[40] J. Besser, J.T. Leito, D.L. van der Meer, C.P. Bagowski, Tip-1 induces filopodia growth and is important for gastrulation movements during zebrafish development, Dev. Growth Differ. 49 (3) (2007) 205–214.
[41] D.L. Ludwig, D.S. Pereira, Z. Zhu, D.J. Hicklin, P. Bohlen, Monoclonal antibody therapeutics and apoptosis, Oncogene 22 (56) (2003) 9097–9106.
[42] R.C. Budd, Death receptors couple to both cell proliferation and apoptosis, J. Clin. Investig. 109 (4) (2002) 437–441.
[43] E. OR, A. Tirincsi, S.E. Logue, E. Szegezdi, The Janus face of death receptor signaling during tumor immunoediting, Front. Immunol. 7 (2016) 446.
[44] H. Wang, M. Han, W. Whetsell Jr., J. Wang, J. Rich, D. Hallahan, et al., Tax-interacting protein 1 coordinates the spatiotemporal activation of Rho GTPases and regulates the infiltrative growth of human glioblastoma, Oncogene 33 (12) (2014) 1558–1569.
[45] T. Kwon, D.Y. Kwon, J. Chun, J.H. Kim, S.S. Kang, Akt protein kinase inhibits Rac1-GTP binding through phosphorylation at serine 71 of Rac1, J. Biol. Chem. 275 (1) (2000) 423–428.
[46] A.S. Fanning, J.M. Anderson, PDZ domains: fundamental building blocks in the organization of protein complexes at the plasma membrane, J. Clin. Investig. 103 (6) (1999) 767–772.
[47] V.K. Subbaiah, C. Kranjec, M. Thomas, L. Banks, PDZ domains: the building blocks regulating tumorigenesis, Biochem. J. 439 (2) (2011) 195–205.